Nat Hazards
DOI 10.1007/s11069-014-1484-x

ORIGINAL PAPER

Geotechnical hazards assessment on wind-eroded desert embankment in Inner Mongolia Autonomous Region, North China

Chi Li · Hao Huang · Lin Li · Yu Gao · Yunfeng Ma · Farshad Amini

Received: 26 March 2014 / Accepted: 20 October 2014

Abstract Inner Mongolia Autonomous Region is one of the severest desertification areas from wind erosion in North China, and it poses as a potential hazard factor for the slope stability of embankments. As the most common and abundant filler in embankment construction in the desert, Aeolian sandy soil is vulnerable to wind erosion. The embankment is susceptible to suffer from damage and lower slope stability due to wind erosion before placement of surface pavement and erosion resistance materials. The purpose of this paper is to evaluate the influence of wind erosion on the slope stability of embankment through a quantitative analysis of shear strength of Aeolian sandy soil within embankments. Field investigation was conducted to measure the wind field around embankment and the shear strength of Aeolian sandy soil within embankment. The shear strength variation was measured and proposed for a characterization of wind erosion resistance. Then, a model for calculating the progressive wind erosion process was suggested for evaluating the slope stability of wind-eroded embankment through the strength reduction theoretical simulation. The results show that wind erosion resistance of Aeolian sandy soil within embankment tends to increase gradually from slope surface to the core and from the shoulder to the toe. When the embankment suffers from wind erosion along prevailing wind direction, its slope has a much weaker resistance on the windward side. The maximum lateral wind erosion depth is about 0.2 times height of embankment. And factors of safety decrease gradually as wind erosion increases, it has affected the local stability of slope, but the slope global stability is not affected under this given wind erosion condition in this study. If wind erosion increases and wind erosion area expands further, the global stability of slope will be on the hazardous level. The speculative study is discussed between slope stability and geometric size of wind-eroded embankment. When the height of embankment increases and its slope becomes steep, its factor of safety decreases, and its slope stability reduces.

C. Li (✉) · H. Huang · Y. Gao · Y. Ma
College of Civil Engineering, Inner Mongolia University of Technology, Hohhot 010051, China
e-mail: nmglichi@gmail.com

C. Li · L. Li · F. Amini
Department of Civil and Environmental Engineering, Jackson State University, Jackson, MS 39217, USA

Published online: 04 November 2014

The results indicate that embankments in Inner Mongolia Autonomous Region should be designed to be lower and gentler in consideration of wind erosion and also recommend scientific and effective protective measures to prevent further development of wind erosion based on proposed maximum lateral wind erosion depth from this study.

Keywords Geotechnical hazards · Wind erosion · Aeolian sandy soil · Wind erosion resistance · Slope stability

1 Introduction

Wind erosion is an important globalized problem, especially, being an urgent issue to tackle for the highway construction and maintenance in the desert regions (Shehata and Amin 1997; Prince et al. 2007; Warren 2010). The Inner Mongolia Autonomous Region lies in North China, with large desert areas in the western part of this region. The averages of annual temperatures range from −1 to 10 °C, and the annual rainfall is about 50–450 mm. It is one of the strongest desertification areas suffering from the most severe wind erosion in China. Most highways in the region have faced with severe erosion challenges; in many cases, the embankment slope collapse have been reported, and wind erosion hazards have been studied in recent years (Dong et al. 2000; Yang et al. 2005; Yu et al. 2012; Guo et al. 2013).

As the most abundant and cheapest filler, Aeolian sandy soil has been widely used in embankment construction for desert highways. This soil is non-cohesive, mostly made up of fine particles and easily eroded. As strong winds blow over the embankment, the embankment acts as an obstacle to the free path of wind and alters the flow field dynamics and wind field energy (Cooke et al. 1993; Lancaster and Greeley 1990; Liu 1995). The fine particles on slope surface are carried away by the wind constantly. The anti-wind erosion ability of unprotected embankment is affected by the wind field intensity, the geometric size of embankment, the angle between embankment centreline and prevailing wind direction, and particle characteristics of filler. It has more influence factors of erodibility than that in the surface soil such as geometric size. Wind erosion of embankment is three-dimensional, whereas the wind erosion of surface soil is two-dimensional. So, an assessment on anti-wind erosion ability of surface soil usually applied the index of "quality loss", and it shows apparent deficiencies in the assessment of embankment filler (Wu 1987; Luo 2000; Song et al. 2006; Li et al. 2012).

Wind erosion of embankment is affected by filler properties and geometric characteristics such as shape and size of the embankment, surface protection against side slope, and its surrounding environments. Most previous researches have focused on the wind flow field features around the embankment through numerical simulation, aerodynamic theory analysis, wind tunnel test, and field measurements (Frank et al. 1993; Badr and Harion 2005; Li and Gao 2011; Xi and Huang 2013). The results of these studies have indicated that the process of wind erosion strongly depends on local wind flow field features, geometric characteristics of embankment, and soil properties of filler. Erosion resistance ability of filler also plays an important role, but the previous researches mainly concentrated in two aspects. One focused on the surface soil erosion (Bagnold 1943; Bisal and Nielsen 1962; Chepil 1941, 1952, 1954; Woodruff and Siddoway 1965; Chepil and Woodruff 1978; Nickling 1978; Fryrear and Saleh 1993; Leys and McTainsh 1996; Zheng

et al. 2004; USDA-NRCS 2003; USDA-ARS 2008; Zobeck 2013; Tatarko et al. 2013; Wagner 2013). For the surface erosion, it is important to research soil erodibility, quantity loss of soil, sand particle saltation movement, characteristic of wind-eroded sediments, wind erosion prediction, and vegetation and desertification. The other is concerned with the internal erosion of structures. The safety of earthen dams is an example due to internal erosion. The researches are now more focused on the influence of particle size and grading on erosion resistance ability and design of filters to prevent internal erosion (Arulanandan and Perry 1983; Sherard 1972; Indraratna et al. 2011). These results obtained from the research on surface erosion or internal erosion can not be simply used to analyse the erosion resistance ability of embankment and can not obtain the lateral erosion depth and evaluate erosion process. This is an incremental process from surface erosion to internal erosion; at the same time, it will cause the loss of stability and the wind erosion resistance reduction of filler.

The influence of wind erosion on slope stability, the degree of the influence, and its effects on the local or global stability are crucial for embankment in the windy and harsh desert environment. Although embankment slope stability has been widely investigated (Duncan 1996; Griffiths and Lane 1999; Duncan and Wright 2005), relatively few studies on the slope stability of wind-eroded embankment have been reported. Hence, in this investigation, a field study was conducted at YanHuang first-class highway in the Inner Mongolia Autonomous Region of North China. Wind flow field and shear strength of Aeolian sandy soil as the filler of embankment were measured. The shear strength variation is proposed for a characterization of wind erosion resistance, and a model for calculating the progressive wind erosion process is built for evaluating the slope stability of wind-eroded embankment through the strength reduction theoretical simulation. These research results provide important information to understand wind erosion mechanism in the desert embankment, to make a reasonable geotechnical hazards assessment on wind-eroded desert embankment, and further to guide the design of desert highways in long-term security conditions.

2 Aeolian sandy soil properties

Aeolian sandy soil is derived from the aeolian parent materials, and its mineral ingredients are mostly composed of the fine particles. The proportion in which diameters range from 0.25 to 0.1 mm is 80.1 %. The stratification of soil surface is not apparent, because it only exists in organic layer, parent material layer, and the layer lacking of deposition (Zhao et al. 2007). The soil is still in its juvenile stage, located in semi-arid sand soil, drought, extreme arid grassland, desert grassland, and desert zone where there are obvious continental climate, lacking of rain, strong evaporation, variable temperature, and year-round windy (Wu 1987).

Aeolian sandy soil was sampled from the edges of Kubuqi desert which was located in the north of Ordos plateau ridge line in the Inner Mongolia Autonomous Region. During the laboratory tests, physical and mechanical properties were measured. It is non-cohesive and has a fine particle size distribution, and the proportion of fine particles in which particle size is <0.25 mm is 91.7 %. The median or median particle size diameter D_{50} is 0.16 mm. It is uniformly graded with coefficient of uniformity (Cu) of 1.77 and coefficient of curvature (Cc) of 1.05, and the particle size distribution curve is shown in Fig. 1a.

According to the Unified Soil Classification System (USCS) (ASTM D2487-11), the soil is classified as silty sands (SM).The sands are round in shape and hardly have any

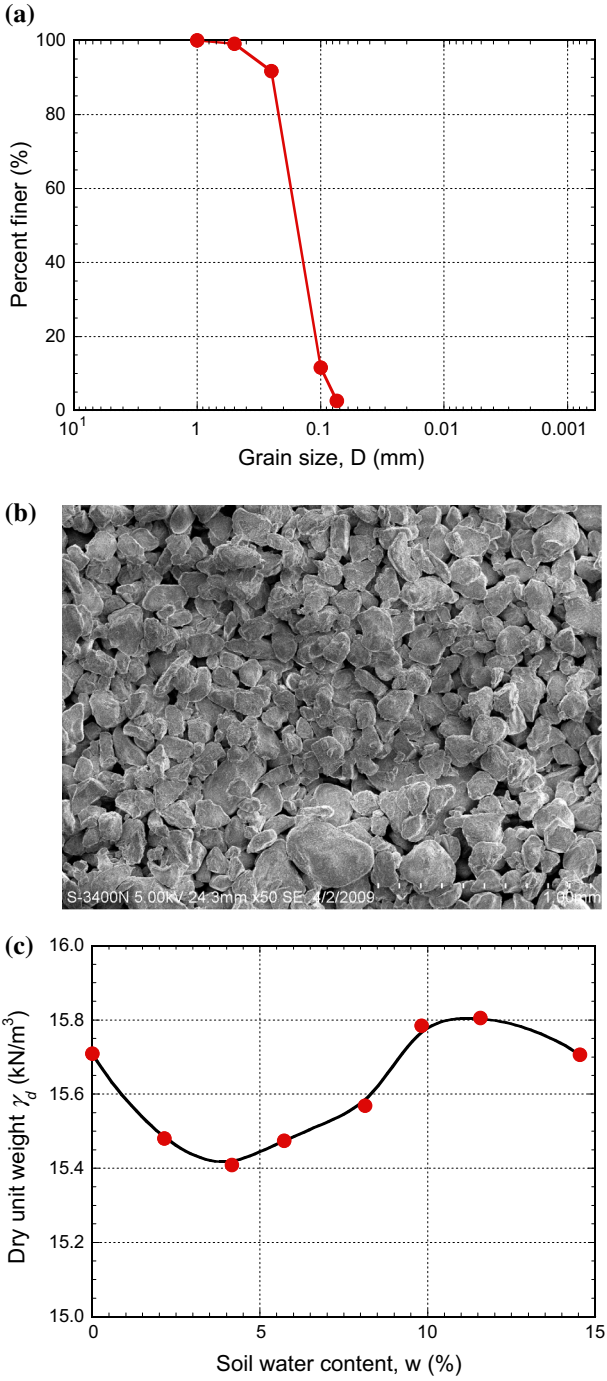

Fig. 1 Aeolian sandy soil properties. **a** Particle size distribution curve. **b** SEM image for particles shape description, and **c** Compaction curve

sharp edges. The shape of the particles is shown in SEM image in Fig. 1b. Figure 1c is the compaction curve of the Aeolian sandy soil in accordance with the standard Proctor compaction test (ASTM D-1557). There are double peaks in the compaction curve, i.e. high dry unit weight (15.7 kN/m^3) at the dry condition and the maximum dry unit weight (15.8 kN/m^3) at the optimum water content of 11 %. The lowest unit weight is 15.4 kN/m^3 at the water content of 4 %. Because of the bimodal phenomena of compaction characteristics, as a filler, Aeolian sandy soil filler is usually operated with dry compaction method in the desert embankment construction sites. The results of unconsolidated-undrained triaxial shear strength test showed that the cohesion and friction angle of Aeolian sandy soil were zero and 18.1°, respectively (Li and Gao 2011; Li et al. 2012). The results of compression test showed that its elastic modulus and Poisson's ratio were 9.4 MPa and 0.25, respectively. It is defined as loose sand (Das 2009). And this soil is often considered as the most easily eroded particles because of the looseness, particle size and shape, grading distribution, and no cohesion between particles (Skidmore and Powers 1982; Skidmore and Layton 1992). Therefore, embankment filled with Aeolian sandy soil is vulnerable to erosion when exposed to wind field. Wind erosion of embankment varies with wind field intensity, geometric size and filler properties of embankment, especially, the angle between embankment centreline and prevailing wind direction. All these will lead to different influences on the slope stability of wind-eroded embankment.

3 Field measuring methods

In the field experiments, wind flow field around embankment and the shear strength of embankment filler in the wind-induced erosion zone were measured. Three measuring sections were selected to illustrate the influence of the angle between embankment centreline and prevailing wind direction. The test sites are located at an Aeolian sandy soil-filled embankment constructed along the YanHuang first-class highway which runs east to west across the Kubuqi desert in the Inner Mongolia Autonomous Region. The Yanhuang first-class highway in different construction processes is shown in Fig. 2, and it is constructed under "Professional Standard of the People's Republic of China (JTG F10-2006)".

The Yanhuang first-class highway is a desert-crossing highway along Kubuqi desert, with an overall length of 420 km and a design speed of 100 km/h. It is divided into three parts: the first part is 111 km from Dalu (K0 + 000) to Shulinzhao (K111 + 000). The second part is 116 km from Shulinzhao (K111 + 000) to Duguitala (K227 + 000). The third part is 171.5 km from Duguitala (K227 + 000) to Balagong (K398 + 500). The remaining parts are connecting line and landscape road. Three measuring sections were selected located in the third part of this newly constructed highway, and they are section K245 + 200, section K240 + 700, and section K239 + 400. The angle between embankment centreline and prevailing wind direction was 90° for section K239 + 400, 60° for section K240 + 700, and 30° for section K245 + 200, respectively. The geographical location of three test sections is shown in Fig. 3a. The embankment has been designed in the crest width of 26 m, height of 3 m, and slope gradient of 1 V:3H. The cross section consists of a 2.0-m-wide medial strip, 2 × 0.75 m wide earth shoulders, 2 × 3.0 m wide hard shoulder, 2 × 0.75 m wide marginal strips, and 4 × 3.75 m wide traffic lanes. The geometric size of embankment is shown in Fig. 3b.

At the test site, the embankment was constructed from October 2009 to April 2010. During the in situ test, the unprotected embankment slope had been exposed to wind erosion environment for 6 months. According to local meteorological data, the annual

Fig. 2 Yanhuang first-class highway in different construction processes: **a** before compaction, **b** after level off and compaction

average wind speed during the last 30 years is 3.8 m/s in April. The maximum wind speed was 20.7 m/s which occurred in April 1980. So, April is the strongest wind season throughout the year. The north-west wind is the prevailing wind direction at the test site. Some meteorological data of Ordos over the past 30 years have been summarized in Fig. 4. The measuring time is in April, 2010, and this desert-crossing highway has been opened in July, 2012. It has become an important highway tunnel between the rich resources region in Ordos and industrial concentration areas.

3.1 Wind flow field surrounding the embankment

Multipoint simultaneous wind speeds were measured. Digital anemometer, which has a maximum wind speed range of 30 m/s, was used. Optical theodolite, sighting rods, and steel tapes were used during the field experiment for taking height and distance measurements.

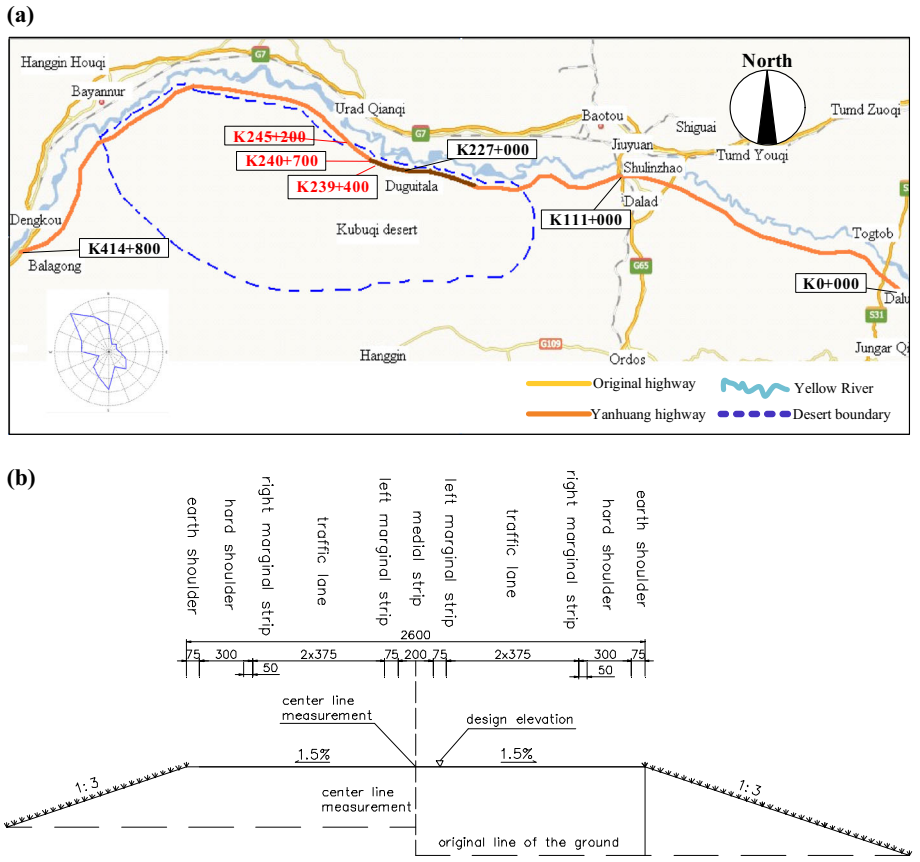

Fig. 3 Some information of the measuring embankment: **a** the geographical location of three measuring sections. **b** The geometric size of embankment and the unit length is m

The locations of wind speed measurement on the embankment and the surrounding area are shown in Fig. 5. With reference to the figure, there are seven measurement locations on the highway embankment, which include the toe of windward slope A, the windward shoulder C, the leeward shoulder E, the toe of leeward slope G, the midpoints of slopes B and F, and the centre of roadway D along embankment cross section. These seven measurement locations are deemed as representative points on the embankment. Wind speed measurements at the selected seven locations were conducted in April, and the average monthly wind speed is 4.2 m/s during this field testing. A reference point was defined at 2 m above the ground surface and 20 H from the toe of the embankment on the windward side, where H is the embankment height. The relative wind speed is computed at each measurement location, and it is a ratio of instantaneous wind speed at each measurement point with that at the reference point at the same time.

The wind speed distribution surrounding the embankment was measured to determine the starting point of wind deceleration in front of the windward side and the point where it regains its original speed on the leeward side. As shown in Fig. 5, twenty locations in front of the windward slope and twenty locations at the back of the leeward slope were selected

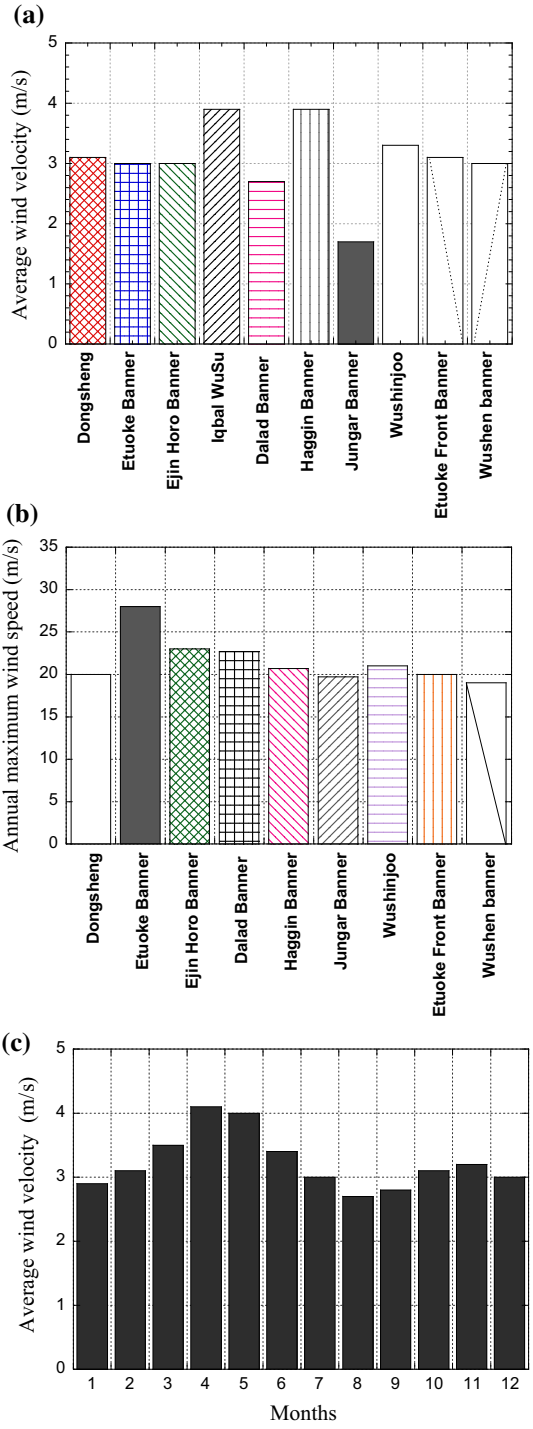

Fig. 4 Meteorological data over 30 years in each banner of Ordos, Inner Mongolia Autonomous Region of North China: **a** average wind speed. **b** Annual maximum wind speed. **c** Average wind speed in 12 months at test site

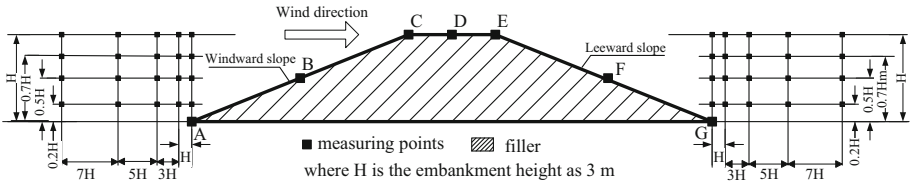

Fig. 5 Wind speed measurement points on the embankment and the surrounding area. The crest width is 26 m, embankment height is 3 m, and slope gradient is 1 V:3H

Table 1 The relative wind speed at different measuring points for section K239 + 400

Trials no.	A	B	C	D	E	F	G
1	0.03	0.57	1.11	0.41	0.93	0.40	0.00
2	0.17	0.68	1.35	0.48	1.13	0.55	0.25
3	0.12	0.51	0.89	0.28	0.48	0.20	0.11
4	0.00	0.60	1.16	0.38	0.74	0.35	0.26
5	0.07	0.56	1.09	0.29	0.71	0.41	0.53
Avg.	0.078	0.584	1.120	0.368	0.798	0.382	0.230
SD	0.0683	0.0627	0.1646	0.0841	0.2449	0.1259	0.1991

Measuring points are shown in Fig. 5

to measure the wind speed during field experiment. The horizontal projected distances of these points from the toe of embankment slope are 1, 3, 5, and 7 H. Their vertical distances from the ground surface are 0.2, 0.5, 0.7 and H, where H is the embankment height (3.0 m in field test). Five readings were taken at each point, and the average value and standard deviation are reported in Table 1. Then, each measurement location and its measuring results are created as the test.grd files. There are three columns in data files, the first two columns data are input with X and Y coordinates, the third column data are the wind speed measurement values. The contour map is built through Golden Software Surfer 8.0, which is shown in Fig. 6a (Golden Software, Inc. 2002).

3.2 Wind erosion resistance of embankment filler

Shear strength of embankment filler is a resistance ability to wind erosion. In this study, the shear strength is more reflected by frictional strength rather than cohesive strength, including slipping friction and rolling friction between sand particles. Shear strength variation of embankment filler is defined and regarded as the characterizing parameter of its wind erosion resistance. First of all, it is challenging to measure the shear strength of cohesionless soil in field test. Before the in situ test was conducted, we had compared different instrumentation and measuring methods. We selected the portable vane shear test method because of the convenience, and it can realize multipoint measurement along the lateral direction from the slope surface to the core. Secondly, these measuring results could be provided for comparison to describe the wind erosion mechanism from surface erosion to internal erosion of desert embankment.

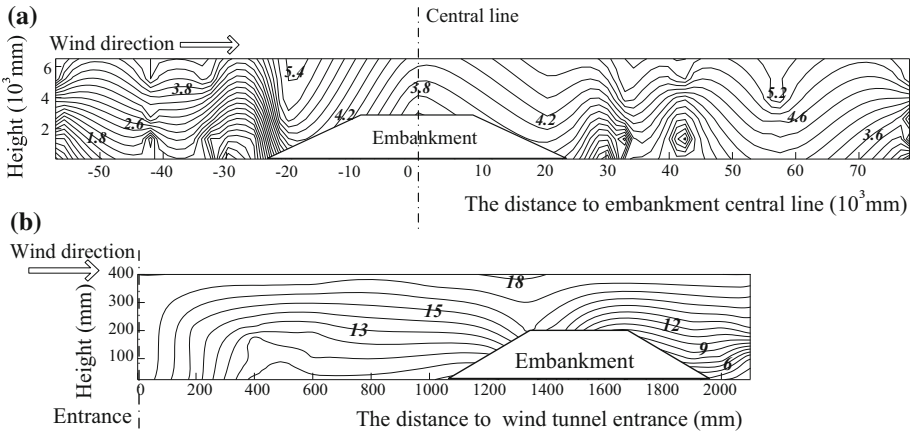

Fig. 6 Wind speed (m/s) distribution surrounding the embankment. **a** Field measuring section K239 + 400 (average monthly wind speed is 4.2 m/s during this field testing, embankment height is 3 m, and slope gradient is 1 V:3H.), and **b** wind tunnel experiment (wind speed is 18 m/s in wind tunnel, embankment model height is 170 mm, and the model slope gradient is 1 V:2H)

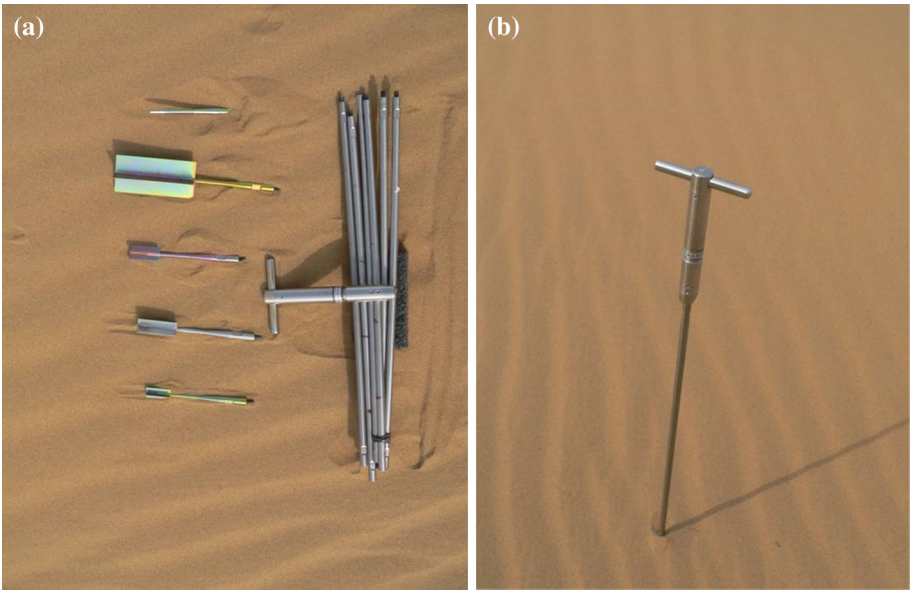

Fig. 7 Field portable vane shear test: **a** apparatus components and **b** test setup

The portable apparatus with a maximum pressure of 260 kPa and a maximum measuring depth of 3.0 m was used. Figure 7 shows the apparatus components and the test setup. Up to six rods, each one measuring 0.5 m in length, were used to reach the 3.0 m depth. The layout of field measuring locations is shown in Fig. 8. The embankment was divided into three horizontal layers of thickness H/3 each. The boundaries of the layers were named (from top to bottom) as the shoulder level, upper level, lower level, and toe

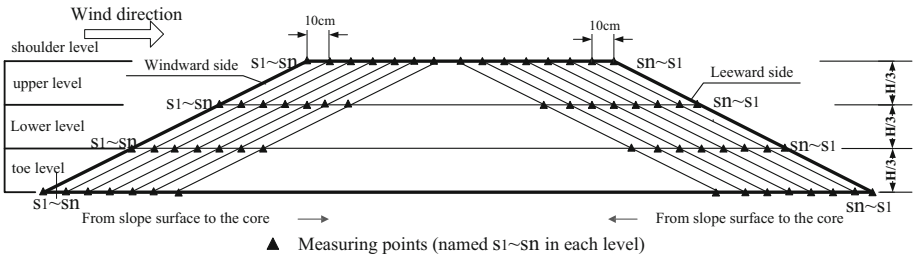

Fig. 8 Layout of field vane shear experiment

level. At each level, the measuring locations were spaced at 10 cm interval along the lateral direction from the slope surface to the core. At each location, the shear strength of soil was measured three times until no variation was found, and the average value is reported.

4 Measuring results and discussion

4.1 Wind flow field surrounding the embankment and erosion mechanism

When the angle between embankment centreline and prevailing wind direction is 90°, it is the strongest disturbed case of natural wind field. In this study, the section K239 + 400 is selected to measure the wind flow field in in situ (Li et al. 2012). The measuring results of wind speeds and calculating results of relative wind speed in section K239 + 400 are summarized in Table 1, and the wind flow distribution surrounding the embankment is shown in Fig. 6a. As shown in Fig. 6a, when the moving wind first encounters the embankment, the wind speed slows down in front of the windward slope, but subsequently, it accelerates gradually along windward slope surface from the toe to the shoulder. After the wind climbs the windward shoulder, it reaches peak speed. Then, the wind starts to decelerate towards the centre of roadway, but once it crosses the centre, it re-accelerates at the leeward shoulder, but its speed at the leeward shoulder is less than at the windward shoulder because the embankment, acting as an obstacle to the free path of wind, causes loss of wind energy. After that, wind speed gradually decreases, reaching its minimum value at the toe of leeward slope. Thereafter, it begins to recover slowly as it moves forward and reaches its original speed. As shown in Table 1, the wind flow field is disturbed and wind speeds at seven locations on the embankment are varied because of the embankment acting as an obstacle. The instantaneous wind speed increases by 12 % on the windward shoulder (point C) and decreases by 77 % at the toe of leeward slope (point G) relative to the instantaneous wind speed at the reference point. From the wind distribution surrounding the embankment, the wind speed begins to slow down at a point approximately 17H (50 m) in front of the toe of windward slope, and it gradually recover its speed as it moves forward, reaching its original speed (4.2 m/s or so) at about 23H (70 m) from the toe of leeward slope.

Li and Gao (2011) conducted wind tunnel experiments to study the wind flow field surrounding the embankment model. The angle between embankment model centreline and prevailing wind direction was 90°, which is same as the section K239 + 400 in field test. An unprotected embankment model was also filled with Aeolian sandy soil. Figure 6b shows the measured wind distribution around an embankment model. Compared with the

results in field measurement, the variation of wind flow field around the embankment model is similar with that is in in situ testing, but the values of wind speed are different. The reasons lie in the two different testing conditions, different starting wind speed, and different geometric size of embankment. From Fig. 6a, b, we draw a wind erosion mechanism based on the wind speed distribution surrounding and on the embankment. It has more influence on wind-induced erosion on the windward side than on the leeward side, and more influence on the upper zone than on the lower zone. Without considering erosion protection for the embankment slope, we speculate about the insufficient wind erosion resistance of Aeolian sandy soil to resist wind erosion on the upper zone of windward side in the embankment.

4.2 Wind erosion resistance of embankment filler and its influence factors

The measured shear strength values of Aeolian sandy soil in the wind-eroded embankment are summarized in Table 2. From Table 2, we can see the field results of three sections as: the section K239 + 400, K240 + 700, and K245 + 200. To better measure the depth of erosion along lateral direction from slope surface to the core, to reduce the influence of soil confining stress, and to describe the shear strength variation of filler due to wind erosion, a characterizing parameter index R_τ, is introduced. It can show the wind erosion velocity of the filler. It also can be assumed to be a variation of shear strength compared to the previous point along the lateral direction from the surface to the core.

The ratio of the velocity of wind erosion Δv_τ of two adjacent points i and $i + 1$ at the same level and the shear strength of point i, τ_i, is defined as a parameter index R_τ, as follows:

$$\Delta v_\tau = \frac{\tau_{i+1} - \tau_i}{l_{i+1} - l_i} \tag{1}$$

$$R_\tau = \frac{\Delta v_\tau}{\tau_i} = \frac{\tau_{i+1} - \tau_i}{\tau_i} \cdot \frac{1}{l_{i+1} - l_i} \tag{2}$$

where τ_{i+1} is the shear strength of point $(i + 1)$; Δv_τ is velocity of wind erosion, it can be described as the variation of shear strength of the filler in this study; l_{i+1}, l_i are measuring depth along lateral for the two adjacent points i and $i + 1$ at the same level; and $(l_{i+1} - l_i)$ is 10 cm in field measurement.

The experimental results from Table 2 were analysed through Eqs. (1) and (2). R_τ is a function of lateral distance from slope surface to the core, as shown in Fig. 9. Figure 9a is the previous measuring results for the section K239 + 400 (Li et al. 2012). Field measurement for the sections K240 + 700 and K245 + 200 are shown in Fig. 9b. From the Fig. 9a, b, the parameter index R_τ decreases as the lateral distance extends from slope surface to the core. R_τ along the windward slope is greater than that in leeward slope for the same lateral extension distance, which is caused by more erosion on the windward side than on the leeward side. Furthermore, R_τ is much higher on the embankment surface than in its interior. It shows that wind erosion is more severe on the slope surface of windward slope. These findings show the consistency in Fig. 9a, b. Summarized field measuring results of different angle between embankment centreline and prevailing wind direction in Fig. 9c. When the lateral extension distance is same, R_τ is relatively bigger at section K239 + 400 and K240 + 700 than at section K245 + 200. This indicates that wind erosion is becoming more serious when the angle between embankment centreline and prevailing wind direction is closer to 90°. Figure 10 shows the relationship between R_τ and

Table 2 Field results of shear strength τ_i at each measuring points

Measuring points and lateral distance		Windward side				Leeward side			
		Toe level	Lower level	Upper level	Shoulder level	Toe level	Lower level	Upper level	Shoulder level
Section		K239 + 400							
S1	0.02	1.2	NA	0.8	NA	1.5	NA	NA	NA
S2	0.17	4.5	1.2	3.3	0.6	5.5	1.5	1.2	0.5
S3	0.27	8.7	4.6	5.8	2.3	11.0	3.3	3.2	3.0
S4	0.37	13.8	7.8	8.8	4.8	16.0	6.2	6.0	5.5
S5	0.47	18.2	11.3	11.9	6.8	21.5	10.2	10.5	10.4
S6	0.57	21.1	12.1	13.7	7.8	23.6	14.5	12.9	13.3
S7	0.67	21.5	12.7	NA	NA	24.1	17.4	15.4	13.9
S8	0.77	NA	NA	NA	NA	NA	18.4	16.3	NA
Section		K240 + 700							
S1	0.02	1.6	1.6	NA	NA	NA	1.6	1.0	0.5
S2	0.17	6.2	5.3	1.6	1.6	5.0	4.0	3.0	2.6
S3	0.27	9.4	8.5	6.0	5.7	11.4	7.8	7.0	7.4
S4	0.37	12.6	11.9	10.6	8.0	19.8	13.1	11.8	12.7
S5	0.47	16.2	15.2	15.0	9.9	25.7	19.6	15.3	13.4
S6	0.57	18.7	17.6	17.7	11.7	29.4	23.6	18.2	13.6
S7	0.67	20.5	18.5	19.3	13.0	30.8	27.6	19.1	NA
S8	0.77	NA	NA	20.3	13.8	32.0	30.0	19.9	NA
S9	0.87	NA	NA	NA	14.5	NA	30.6	NA	NA
Section		K245 + 200							
S1	0.02	NA	2.5	2.5	NA	2.0	2.0	1.2	0.5
S2	0.17	5.0	8.6	5.9	2.5	6.7	7.1	5.8	2.7
S3	0.27	12.3	14.7	9.3	6.6	12.7	10.6	11.3	6.5
S4	0.37	20.5	21.3	12.9	7.9	20.6	14.4	15.9	8.3

Table 2 continued

Measuring points and lateral distance		Windward side				Leeward side			
		Toe level	Lower level	Upper level	Shoulder level	Toe level	Lower level	Upper level	Shoulder level
S5	0.47	27.9	27.1	15.6	9.1	25.9	18.1	18.8	9.5
S6	0.57	30.4	29.5	16.3	10.2	30.6	21.0	19.7	10.7
S7	0.67	30.7	NA	NA	10.7	31.2	22.5	NA	11.2

NA not available

The field measuring points are located in Fig. 8

The unit of shear strength τ_i is kPa. The unit of lateral distance is *m*

The first measuring point locates in a distance of 0.02 m from slope surface and the measuring depth which is a requirement of the experimental apparatus. Other points are set at every 0.1 m along the lateral direction from slope surface to the core and added with a distance of plate thickness 0.05 m at every measuring point

lateral distance from slope surface to the core obtained from the wind tunnel experiment (Li and Gao 2011). The variation of R_τ versus lateral distance is compared between the field measuring results and the wind tunnel test results. It shows a similar variation trend both in wind tunnel test and in field measurement despite two different stress states. It also decreases as the lateral distance extends from slope surface to the core. It is greater on shoulder level than that on the upper level for the same lateral extension distance.

The critical boundary of wind erosion area can be found by determining the turning point of shear strength variation and its location. The curves of "R_τ versus lateral distance from slope surface to the core" are summarized in Fig. 9a, b, c. From the Fig. 9, R_τ decreases and gradually approaches zero, as the distance increases from the slope surface to its core. The lateral erosion depth is defined as a horizontal projected distance from turning point, which tends to level off from steepness in the curve as shown in Fig. 9. The lateral erosion depths at the four testing levels at the three field test sections are summarized in Table 3. The maximum depth was 0.57 m, and occurred on the shoulder along windward side at section K239 + 400, and the minimum depth was 0.17 m, which occurred on the toe of leeward side at section K245 + 200. The results show that the ability to resist wind erosion is weaker on the upper level of windward side than on the lower level of leeward side. Through the field measurements, we found the maximum lateral erosion depth is approximately 0.2 H (H is the embankment height) on the shoulder along windward side for the given desert environment as described in this paper.

5 An assessment on slope stability of wind-eroded embankment

5.1 Theoretical calculation method

As we know, wind erosion damage to sands mainly manifests itself in the form of slipping and rolling between particles, particles hopping in ballistic trajectories close to the ground, and ejecting new particles upon collision with the bed (Bagnold 1943). When the external force due to wind is strong enough to overcome friction between particles, the particles begin slipping, rolling, and hopping, at this time, wind erosion occurs (Leon 1988).

We have a hypothesis that when particles of cohesionless soil begin to roll or slide due to wind erosion, friction forces between particles act as the resistance. At this point, the erosion mechanism is the same between water erosion and wind erosion, and the critical stress state is linearly related to the particle diameter (White 1940; Briaud et al. 2007). A mechanism model of rolling or sliding between particles has been built, and the friction forces among particles satisfy the equilibrium requirements as in Eq. (3). Equation (4) which is derived from Eq. (3) shows the relationship between friction angle and the shear strength for cohesionless soil at its wind erosion critical state. From the Eq. (4), we can see that τ_c is shear strength at critical state, it can be determined by analysing the measuring results of field vane shear test, which is shown in Table 2, and ϕ_c is the critical friction angle at wind erosion critical state, it can be determined through Eq. (4). This theoretical calculation method has been verified, and the details have been demonstrated in Li et al. 2012.

$$\tau_c A_e = W \tan \varphi_c \tag{3}$$

$$\varphi_c = \tan^{-1}(3\alpha\tau_c / 2\rho_s g D_{50}) \tag{4}$$

where A_e is the effective contact area between particles; α is the ratio of effective area over the maximum cross section of the spherical particle; it is usually taken as 1/3; ρ_s is the

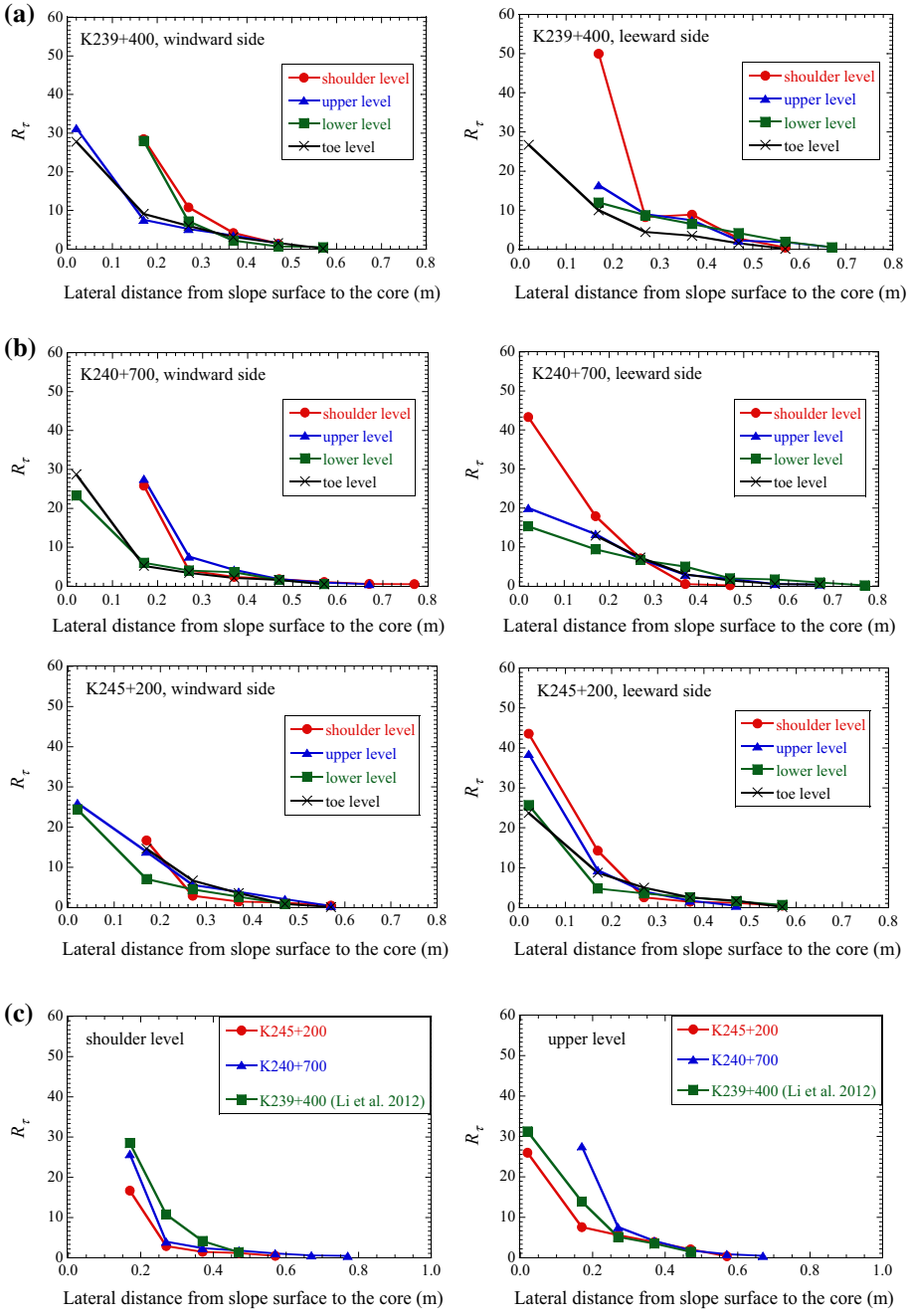

Fig. 9 R_τ varies with lateral distance from slope surface to the core in field measuring: **a** for section K239 + 400 (Li et al. 2012), windward side and leeward side; **b** for section K240 + 700 and section K245+200, windward side and leeward side; **c** for different angle between embankment centreline and wind direction, shoulder level and upper level

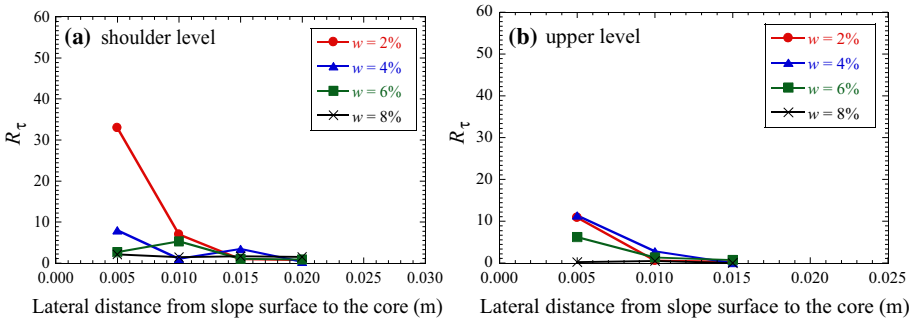

Fig. 10 R_τ varies with lateral distance from slope surface to the core in wind tunnel experiment for windward side with different soil moisture content **a** shoulder level and **b** upper level (tunnel wind speed was 10 m/s, blowing for 40 min) (Li and Gao 2011)

Table 3 Lateral erosion depth of four testing levels at three field test sections

Section	Testing level	Windward side (m)	Leeward side (m)
K239 + 400	Toe level	0.47	0.37
	Lower level	0.47	0.47
	Upper level	0.47	0.47
	Shoulder level	0.57	0.47
K240 + 700	Toe level	0.37	0.27
	Lower level	0.37	0.27
	Upper level	0.47	0.37
	Shoulder level	0.47	0.37
K245 + 200	Toe level	0.27	0.17
	Lower level	0.37	0.27
	Upper level	0.37	0.37
	Shoulder level	0.47	0.37

mass density of particles; D_{50} is mean diameter representative of the soil particle size distribution; and g is the acceleration due to gravity.

For the windward slope of embankment, the critical friction angles of Aeolian sandy soil can be obtained using Eq. (4), and the results are summarized in Table 4. As shown in this table, the critical friction angle gradually increases and approaches to the original internal friction angle of soil (18.1°) from slope surface to the core and from the shoulder level to the toe level.

5.2 Numerical simulation and assessment on slope stability for wind-eroded embankment

The finite element program ABAQUS was used to evaluate the slope stability of wind-eroded embankment (ABAQUS 2002). The strength reduction method was used to evaluate the slope stability, and the factor of safety *F.S.* was suggested as an evaluation index of slope stability for wind-eroded embankment (Duncan 1996; Duncan and Wright 2005).

Table 4 Critical friction angles of soil in wind erosion areas for different sections

Measuring points and lateral distance		Windward side			
		Toe level	Lower level	Upper level	Shoulder level
Section		K239 + 400			
S1	0.02	1.2	NA	0.8	NA
S2	0.17	4.6	1.2	3.4	0.5
S3	0.27	9.0	4.7	6.0	2.3
S4	0.37	14.8	8.1	9.1	4.9
S5	0.47	20.3	11.9	12.6	7.0
S6	0.57	24.4	12.8	14.7	8.9
S7	0.67	25.0	13.5	NA	NA
S8	0.77	NA	NA	NA	NA
Section		K240 + 700			
S1	0.02	1.6	1.6	NA	NA
S2	0.17	6.4	5.4	1.6	1.6
S3	0.27	9.8	8.8	6.2	5.8
S4	0.37	13.4	12.6	11.1	8.3
S5	0.47	17.7	16.5	16.2	10.3
S6	0.57	21.0	19.5	19.7	12.4
S7	0.67	23.5	20.7	21.8	13.8
S8	0.77	NA	NA	23.2	14.8
S9	0.87	NA	NA	NA	15.6
Section		K245 + 200			
S1	0.02	NA	2.6	2.6	NA
S2	0.17	5.1	8.9	6.1	2.6
S3	0.27	13.0	15.9	9.7	6.8
S4	0.37	23.5	24.7	13.7	8.2
S5	0.47	36.0	34.5	17.0	9.5
S6	0.57	41.4	39.4	17.9	10.7
S7	0.67	42.1	NA	NA	11.2

NA not available

The measuring points of the field vane shear test are located in Fig. 8

The unit of critical friction angle is °. ϕ is calculated through Eq. (4). Critical friction angle may be greater than the inner friction angle of soil around the core, because of the lateral restriction of soil

As you know, *F.S.* is closely associated with strength reduction failure criteria. Usually, there are three failure criteria. The first one is no convergence in finite element numerical (FEM) calculation. The other two are the plastic zone connected from the toe to the top of slope and displacement unlimited development of one point on the slip surface (Griffiths and Lane 1999; Luan et al. 2003; Zienkiewicz et al. 1975; Duncan and Chang 1970). In this article, the failure criteria of no convergence in FEM calculation is used, and unlimited development of displacement is taken into consideration in the process. If the point appears, the calculation is stopped. The strength reduction failure criteria in FEM calculation is adopted for evaluation on stability of embankment slope. When the *F.S.* is <1.0, the side slope will lose its global stability, and the embankment may collapse in a moment.

When the *F.S.* is more than 1.0 and <1.3, the side slope of embankment is taken as being unstable, and the local stability is on the hazardous level. When the *F.S.* is >1.30, the side slope of embankment is taken as being stable (Professional Standard of the People's Republic of China (JTG D30-2004)).

The numerical model in the simulation has the same geometric size as that of embankment in the YanHuang first-class highway. Only the windward side of embankment is considered in slope stability analysis for the section K239 + 400. The properties of Aeolian sandy soil are used in the slope stability model. The dry unit weight is 15.7 kN/m^3, the cohesion is zero, the friction angle is 18.1°, and the dilation angle is same as the friction angle. The elastic modulus and Poisson's ratio are 9.4 MPa and 0.25, respectively. The Mohr–Coulomb yield criterion is assumed in simulation. For the desert embankment filling with Aeolian sandy soil, the *F.S.* equals to 1.36 with non-erosion condition based on the FEM calculation. The wind erosion areas are divided into 17 cells. Each cell has a width of 0.15 m and a height of 0.75 m and is subjected to different wind erosion scenarios. Table 5 shows the cell locations and different wind erosion scenarios. All wind erosion scenarios start from the shoulder of the windward side. Taking "(e), 1 → 4" scenarios, for example, the wind erosion areas expand gradually as the cell develops from 1 → 2 → 3 to 4, which is shown in Table 5. The lateral width of wind erosion areas is 0.3 m, and the vertical height is 1.5 m. The wind erosion areas on windward side of section K239 + 400, the measurement locations of friction angle are set from shoulder level to upper level, from S_1 to S_3 along lateral direction, as shown in Table 4. The relationship is built between wind erosion areas and friction angle through the measurement locations and its distance combining Tables 4 and 5. For the cells 1 and 3, the distance is 0.3 m on the shoulder level, corresponding to the measurement location is from S_1 to S_2 and from S_2 to S_3, respectively. Then, the average value of friction angle corresponding to the measurement location from S_1 to S_2 is assigned to cell 1, and the average value of friction angle corresponding to the measurement location from S_2 to S_3 is assigned to cell 3. The same procedure is conducted on the cell 2 and 4 on the upper level. In this way, the average value of friction angle from cell 1 to cell 4 is 0.5°, 2.1°, 1.4°, and 4.7°, respectively. And other cells which are not affected by wind erosion are set in 18.1°. At this wind erosion scenario, the *F.S.* is 1.34 based on the FEM calculation.

This method reflects a progressive wind erosion process. For a given condition of wind erosion on the windward side, the factor of safety can be obtained for eighteen cases using areas affected by seventeen different degrees of wind erosion, and one case which is not affected by wind erosion. The numerical results are shown in Table 5. As shown in Table 5, the slope stability of wind-eroded embankment can be affected when the wind erosion area extends and generates a connected surface as indicated by the dotted line. When wind erosion areas extend gradually from the connected surface to the core and from the shoulder to the toe, the factor of safety decreases according to different failure stage, from stable to unstable scenarios going through different wind erosion influence zone, the shoulder, upper, lower, and toe level. But the slope global stability of embankment is not affected, it is just a local instability. If wind erosion continues and wind erosion area expands further, the global stability of the slope will be on the hazard. Afterwards, the relationship is discussed between slope stability of wind-eroded embankment and geometric size of embankment. The factor of safety for different embankment heights and different slope gradients are simulated and listed in Table 5. When the height of embankment increases and the slope steepens, the wind flow field is disturbed noticeably and the wind erosion is enhanced on the windward slope. In this case, the factor of safety decreases and the slope becomes gradually less stable. From the Table 5, when the slope gradient is 1 V: 3H, the factor of safety is ≥1.30, so the slope is stable for the height

Table 5 Factor of safety *F.S.* for different wind erosion scenarios and its influence factors

Schematic diagram	Wind erosion areas		Wind erosion scenarios	*FS*
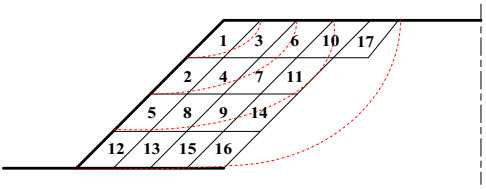	Stable	(*a*)	Non-erosion	1.36
	Shoulder	(*b*)	"1"	1.36
		(*c*)	"1→2"	1.36
		(*d*)	"1→3"	1.34
	Upper	(*e*)	"1→4"	1.34
		(*f*)	"1→5"	1.34
		(*g*)	"1→6"	1.34
		(*h*)	"1→7"	1.34
		(*i*)	"1→8"	1.34
	Lower	(*j*)	"1→9"	1.32
		(*k*)	"1→10"	1.32
		(*l*)	"1→11"	1.32
		(*m*)	"1→12"	1.32
		(*n*)	"1→13"	1.32
		(*o*)	"1→14"	1.30
	Toe	(*p*)	"1→15"	1.30
		(*q*)	"1→16"	1.30
		(*r*)	"1→17"	1.28

F.S. versus different geometric size

Height (m)	Slope gradient		
	1V:3H	1V:2H	1V:1.75H
1.0	1.40	1.35	1.32
1.5	1.37	1.32	1.29
2.0	1.32	1.28	1.25
2.5	1.31	1.26	1.23
3.0	1.30	1.25	1.22

≤3.0 m. At the other two kinds of slope gradient, embankment height should be <2 m, and in this case, wind erosion damage on the slope stability of embankment is weak. Above all, we can gain some insights from these findings to guide the design of desert highways, it should be designed with lower and gentler when the influence of wind erosion is considered, embankment height should be <2 m, and the better slope gradient is slower than 1 V: 3H, to avoid causing the serious disturbance of wind field surrounding the embankment.

6 Conclusions

A geotechnical hazards assessment on wind-eroded desert embankment was conducted. Wind field distribution around the embankment and wind erosion resistance of the filler

were measured in in situ. Some efforts were also made to study the erosion mechanism of wind-eroded embankment and its slope stability and to verify the correlation between the laboratory findings and field measurements. The anti-wind erosion ability of embankment filler is more complex than that of surface soil and has more influence factors. It is a progressive wind erosion process for embankment slope. Field measurements show that the ability to resist wind erosion increases gradually from slope surface to the core, and it decreases gradually from the toe to the shoulder. So, the slope stability gradually decreases as wind erosion extends from slope surface to the core and from the shoulder to the toe. When the angle closes to 90°, the ability to resist wind erosion is weaker than other angles. The maximum lateral erosion depth is about 0.2 times height of the embankment from these measuring results. In this paper, the approach is creative, and it can be well applied to research wind erosion mechanism of other earthen structures. These approaches to reveal wind erosion mechanism and prevent wind erosion development are original ideas based on the theories of geotechnical engineering. Of course, there are limitations in this study. Aeolian sandy soil is taken from the edges of Kubuqi desert, Ordos plateau, Inner Mongolia Autonomous Region of North China. It can represent the typical grain size distribution in the Inner Mongolia area, but it may not represent the typical characteristics in other areas in China or in other part of the world. The findings obtained from the field measurements along Yanhuang first-class highway present a wind erosion mechanism although there are still imperfections in field measurements, and they need to be improved in subsequent research. As a measuring method, it is not the best, but it is quite a "portable instrumentation" suitable for measurement in the desert, and the measuring results could be provided for comparison to describe wind erosion mechanism from surface erosion to internal erosion of desert embankment.

Acknowledgments The authors acknowledge the support provided by the Natural Science Foundation of China (NO. 50868010, 51168035) and by the program for New Century Excellent Talents at the University of Ministry of Education of China (NCET-11-1016) and Young Talents of Science and Technology at the Universities of Inner Mongolia Autonomous Region (YTST). The first author also thanks the China Scholarship Council for providing support for a 1-year visiting study to the United States. In addition, the project management unit of YanHuang first-class highway in Ordos, Inner Mongolia Autonomous Region of North China is gratefully acknowledged for their generous assistance during the field experiment.

References

ABAQUS (2002) ABAQUS user's manual, Version 6.2. Hibbit, Karlson & Sorenson, Inc., Pawtucket, Rhode Island

Arulanandan K, Perry EB (1983) Erosion in relation to filter design criteria in earth dams. J Geotech Energy 109:682–698

Badr T, Harion JL (2005) Numerical modeling of flow over stockpiles: implications on dust emissions. Atmos Environ 39:5576–5584

Bagnold RA (1943) The physics of blown sand and desert dunes. Meghuen, London

Bisal F, Nielsen KF (1962) Movement of soil particles in saltation. Can J Soil Sci 142:81–86

Briaud JL, Chen HC, Govindasamy AV, Storesund R (2007) Erosion tests on samples from New Orleans levees. Geo-Denver: New Peaks in Geotechnics, GSP161 Embankments, Dams, and Slopes

Chepil WS (1941) Relation of wind erosion to the dry aggregate structure of a soil. Sci Agric 21:488–507

Chepil WS (1952) Factors that influence clod structure and erodibility of soil by wind: soil structure. Soil Sci 75:473–483

Chepil WS (1954) Factors that influence clod structure and erodibility of soil by wind: sand silt and clay. Soil Sci 80:155–162

Chepil WS, Woodruff NP (1978) Sedimentary characteristics of dust storms: II. Visibility and dust concentration. Am J Sci 255:104–114

Cooke R, Warren A, Goudie A (1993) Desert Geomorphology. UCL Press
Das BM (2009) Principles of geotechnical engineering. Cengage Learning, Stamford
Dong ZB, Wang XM, Liu LY (2000) Wind erosion in arid and semiarid China: an overview. J Soil Water Conserv 55(4):439–444
Duncan JM (1996) State of the art: limit equilibrium and finite element analysis of slope. J Geotech Eng ASCE 122(7):577–596
Duncan JN, Chang CY (1970) Nonlinear analysis of stress and strain in soils. J Soil Mech Found Div Eng ASCE 56(SM5):1625–1653
Duncan JM, Wright SG (2005) Soil strength and slope stability. Wiley, New Jersey
Frank H, Heldt K, Emeis S, Fiedler F (1993) Flow over an embankment: speed-up and pressure perturbation. Bound-Layer Meteorol 63(1):163–182
Fryrear DW, Saleh A (1993) Field wind erosion: vertical distribution. Soil Sci 155(4):294–300
Golden Software, Inc. (2002) Surfer 8 user's guide. Golden Software, Inc., Golden, Colorado
Griffiths DV, Lane PA (1999) Slope stability analysis by finite elements. Geo-technique 49(3):387–403
Guo Z, Zobeck TM, Zhang K, Li F (2013) Estimating potential wind erosion of agricultural lands in northern China using the Revised Wind Erosion Equation and geographic information systems. J Soil Water Conserv 68(1):13–21
Indraratna B, Nguyen TV, Rujikiatkamjorn C (2011) Assessing the potential of internal erosion and suffusion of granular soils. J Geotech Geoenviron Eng 137:550–554
Lancaster N, Greeley R (1990) Sediment volume in the north polar sand seas of Mars. J Geophys Res 95:921–927
Leon L (1988) Basic wind erosion processes. Agric Ecosyst Environ 22(23):91–101
Leys JF, McTainsh GH (1996) Sediment fluxes and particle grain-size characteristics of wind-eroded sediments in southeastern Australia. Earth Surf Process Landforms 21:661–671
Li C, Gao Y (2011) Experimental studies on wind erosion mechanism of aeolian soils subgrade slope for desert highway. Adv Mater Res 243–249:2401–2408
Li C, Ge X, Huang H (2012) Study on wind erosion resistance ability and slope stability of wind-eroded desert roadbed. Forensic Eng, 746–754
Liu XW (1995) Experimental aeolian sand physics and engineering. Science Press, Beijing, China. (In Chinese)
Luan MT, Wu JJ, Nian TJ (2003) A criterion for evaluating slope stability based on development of plastic zone by shear strength reduction FEM. J Disaster Prev Mitig Eng 23(3):1–8 (In Chinese)
Luo JB (2000) Study on techniques and its mechanism for controlling sand hazard to highway in different type regions of desert in China. Ph.D Thesis for Beijing Forestry University. (In Chinese)
Nickling WG (1978) Aeolian sediment transport during dust storms: Slims River Valley, Yukon Territory. Can J Earth Sci 15:1069–1084
Prince SD, Wessels KJ, Tucker CJ, Nicholson SE (2007) Desertification in the Sahel: a reinterpretation of a reinterpretation. Glob Change Biol 13(7):1308–1313
Professional Standard of the People's Republic of China (JTG D30-2004). Specifications for design of highway subgrades. China Communications Press, Beijing, China. (In Chinese)
Professional Standard of the People's Republic of China (JTG F10-2006). Technical specifications for construction of highway subgrades. China Communications Press, Beijing, China. (In Chinese)
Shehata WM, Amin AA (1997) Geotechnical hazards associated with desert environment. Nat Hazards 16:81–95
Sherard JL (1972) Study of piping failure and erosion damage from rain in clay dams in Oklahoma and Mississippi. Soil Conservation Service, Washington
Skidmore EL, Layton JB (1992) Dry-soil aggregate stability as influenced by selected soil properties. Soil Soc Am J 56:557–561
Skidmore EL, Powers DH (1982) Dry–soil aggregate stability: energy-based index. Soil Sci Soc Am J 46(6):1274–1279
Song Y, Liu LY, Yan P, Cao T (2006) A review of soil erodibility research. Arid Land Geogr 29(1):124–131 (In Chinese)
Tatarko J, Sporcic MA, Skidmore EL (2013) A history of wind erosion prediction models in the United States Department of Agriculture prior to the Wind Erosion Prediction System. Aeolian Res 10:3–8
USDA-ARS (2008) The wind erosion prediction system: WEPS 1.0 User Manual. USDA–ARS Wind Erosion Research Unit, Manhattan, USA
USDA-NRCS (2007) Web Soil Survey, Version 2.0. USDA, Natural Resource Conservation Service
Wagner LE (2013) A history of wind erosion prediction models in the United States Department of Agriculture: the wind erosion prediction system (WEPS). Aeolian Res 10:9–24
Warren A (2010) Sustainability in aeolian systems. Aeolian Res 1:95–99

White CM (1940) The equilibrium of grains on the bed of a stream. Proc R Soc Lond 174(958):322–338
Woodruff NP, Siddoway FH (1965) A wind erosion equation. Soil Sci Soc Am Proc 29(5):602–608
Wu Z (1987) Aeolian sand geomorphology. Science Press, Beijing, China. (In Chinese)
Xi CG, Huang TH (2013) Road domain near-surface wind movement characteristics in sandy area. J Highw Transp Res Dev 7(3):30–36
Yang X, Zhang K, Jia B, Li C (2005) Desertification assessment in China: an overview. J Arid Environ 63(2):517–531
Yu XX, Qi SZ, Xu YT (2012) Soil erosion hazard in the Yimeng mountainous region, North China. Nat Hazards 64:1963–1967
Zhao HL, Zhou RL, Drake S (2007) Effects of aeolian deposition on soil properties and crop growth in sandy soils of Northern China. Geoderma 142(3–4):342–348
Zheng XJ, He LH, Zhou YH (2004) Theoretical model of the electric field produced by charged particles in windblown sand flux. J Geophys Res 109:D15208
Zienkiewicz OC, Humpheson C, Lewis RW (1975) Associated and non-associated visco-plasticity and plasticity in soil mechanics. Geotechnique 25(4):671–689
Zobeck TM (2013) Soil property effects on wind erosion of organic soils. Aeolian Res 10:43–51